Available online at www.sciencedirect.com
SCIENCE DIRECT®
Journal of Magnetic Resonance 176 (2005) 207–214
JMR Journal of Magnetic Resonance
www.elsevier.com/locate/jmr

Optically detected nuclear magnetic resonance at the sub-micron scale

Carlos A. Meriles *

Department of Physics, City College of New York—CUNY, New York, NY 10031, USA

Received 28 March 2005; revised 24 May 2005
Available online 21 July 2005

Abstract

Nuclear magnetic resonance is arguably one of the most powerful techniques available today to characterize diverse systems. However, the low sensitivity of the standard detection method constrains the applicability of this technique to samples having effective dimensions not less than a few microns. Here, we propose a novel scheme and device for the indirect detection of the nuclear spin signal at a submicroscopic scale. This approach—for which the name Dipolar Field Microscopy is suggested—is based on the manipulation of the long-range nuclear dipolar interaction created between the sample and a semiconductor tip located close to its surface. After a preparation interval, the local magnetization of the sample is used to modulate the nuclear magnetization in the semiconductor tip, which, in turn is determined by an optical inspection. Based on results previously reported, it is shown that, in principle, images and/or localized high-resolution spectra of the sample can be retrieved with spatial resolution proportional to the size of the tip.

Keywords: NMR microscopy; Dipolar fields; Optical detection; Hyperpolarization; Micro-tips; Dipolar Field Microscopy

1. Introduction

One of the most important challenges in modern nuclear magnetic resonance (NMR) is the study of systems with spatial resolution less than $\sim$10 μm. This difficulty derives basically from the fact that, in conventional NMR, the signal-to-noise ratio is proportional to the nuclear magnetic polarization of the sample. Despite steady progress in the construction of stronger superconducting magnets, this polarization is only a small fraction of the attainable maximum ($\sim 10^{-4}$ for protons in a 14 T magnet) so, typically, 10^{16}–10^{18} molecules are necessary for meaningful measurements. Also, in "traditional" NMR, the detected signal results from Faraday induction in the coil surrounding the sample. Compared to other detection methods, the sensitivity of this scheme is rather poor since, even with maximum polarization, the minimum number of spins needed to induce a measurable signal is invariably large.[1]

Given the growing interest in studying systems at submicroscopic scales, various methods have been implemented to mitigate these problems. In semiconductors, for example, irradiation via circularly polarized light or "optical pumping" makes it possible to reach a nuclear alignment of up to 70% [2]. This effect leads to the generation of an effective magnetic field acting on the semiconductor electrons, which, in turn, can be used to optically determine the nuclear polarization with exquisite sensitivity [3]. Although various methods have been used in the past to optically probe the nuclear alignment [3,4], here we will pay particular attention to schemes based on Faraday rotation [5,6]. In this case, the electronic Larmor frequency within the

* Fax: +1 212 650 6940.
E-mail address: cmeriles@sci.ccny.cuny.edu.

[1] Near field optical microscopy serves as a useful reference for comparison. See, for instance [1].

1090-7807/$ - see front matter © 2005 Elsevier Inc. All rights reserved.
doi:10.1016/j.jmr.2005.05.023

semiconductor is determined by recording the temporal change in the linear polarization of a time-delayed "probe" pulse following a stronger (circularly polarized) "pump" pulse. When the system has been previously hyperpolarized, the nuclear alignment alters (through the hyperfine coupling) the effective magnetic field acting on the electrons. Thereby, the nuclear polarization can be determined by comparing the measured precession frequency with the one exclusively due to the external magnetic field. This scheme has a remarkable sensitivity and has been used to reconstruct nuclear magnetic resonance spectra in minuscule regions of a semiconductor [7].

This manuscript introduces a novel scheme for the ultra-sensitive detection of nuclear magnetic resonance in samples of arbitrary composition, with emphasis on those of biological relevance (protonated systems). With this purpose, the use of a hyperpolarized semiconductor tip placed close to the surface of an extended sample will be discussed. In this geometry, it will be first shown that it is possible to use the tip dipolar field to select a region of interest within the sample. This is a versatile process with multiple alternatives. However, the most interesting case is the one in which the sample magnetization is restricted to a small region of volume proportional to the size of the tip. This sharply inhomogeneous distribution of magnetization is used, in a second step, to modulate the amplitude of the nuclear magnetization in the tip. As explained below, an optical reading makes it possible to indirectly get local information on the sample with sensitivity (almost) independent of its polarization. Based on experimental results previously reported by other groups, it will be also shown that, in principle, it is possible to reconstruct images and obtain high-resolution spectra with a spatial discrimination comparable to the size of the tip.

Let us consider the setup in Fig. 1: an intense external magnetic field uniformly polarizes an extended sample in the direction perpendicular to its surface. Close to this surface is a semiconductor tip previously hyper-polarized by optical pumping (with either a cw or pulsed circularly polarized laser beam). The setup also includes a radio-frequency (RF) coil to manipulate the evolution of the spin system in the sample and in the tip. For simplicity, it has been assumed that the hyperpolarized region is spherical[2] with radius a, and that its center is located a distance d from the surface of the sample. In this case, the tip induces a dipolar magnetic field of the form

$$\mathbf{B}_{\text{tip}} = \frac{\mu_0}{3r'^3}\left(\frac{a}{d}\right)^3 (3(\mathbf{M}^{(0)}_{\text{tip}} \cdot \hat{\mathbf{r}}')\hat{\mathbf{r}}' - \mathbf{M}^{(0)}_{\text{tip}}). \quad (1)$$

$\mathbf{M}^{(0)}_{\text{tip}}$ represents the (pumped) nuclear magnetization in the tip (collinear with the external field) μ_0 is the vacuum magnetic permeability and $\mathbf{r}'$ is the vector from the sample to the center of the sphere; the prime indicates that the coordinates have been expressed in units of the distance d. The spatial variation of the dipolar field can be used to select the sample region to be studied. Let us consider, for instance, the RF pulse sequence $(\pi/2)_y - t_{c1} - (\pi/2)_x$ acting on the sample nuclei. As usual in NMR, the sub-index in each pulse indicates the RF phase in the rotating frame; t_{c1} represents the variable evolution interval between the pulses. If for now we do not take into account spin interactions other than the long-range dipolar field between the sample and the tip (i.e., J-couplings, homo- or heteronuclear dipolar interactions within the sample or tip, chemical shifts, etc.), a simple calculation shows that, at the end of the sequence, the magnetization along the z-direction (parallel to the external magnetic field) is given by

$$\mathbf{M}^{(z)}_{\text{spl}}(t_{c1}) = \mathbf{M}^{(0)}_{\text{spl}} \sin(\gamma_{\text{spl}} t_{c1} (B_{\text{tip}})_z). \quad (2)$$

$\mathbf{M}^{(0)}_{\text{spl}}$ represents the equilibrium magnetization in the sample and γ_{spl} is the nuclear gyromagnetic ratio of the probed nuclei. Finally, $(B_{\text{tip}})_z = (B^{\max}_{\text{tip}}/2r'^5)(3z'^2 - r'^2)$ is the z-component of the dipolar field due to the tip in primed coordinates; $B^{\max}_{\text{tip}} = (2\mu_0/3)M^{(0)}_{\text{tip}}(a/d)^3$ is the maximum value of this field over the sample.

The use of the dipolar field due to the tip to control the distribution of magnetization in the sample can be directly visualized in Fig. 2. In case A, the inter-pulse interval t_{c1} has been chosen such that $\gamma_{\text{spl}} t_{c1} B^{\max}_{\text{tip}} = \pi/2$. The result is the concentration of magnetization in the region closest to the tip. As inferred from the figure, this volume is basically proportional to d^3 indicating that the magnetization becomes more localized as the center of the hyperpolarized sphere moves closer to the sample surface. Reciprocally, the sharply inhomogeneous distribution of the sample magnetization induces a strong long-range dipolar field at the tip. Fig. 3 shows a field map in the region close to its center (of curvature); notice that the dipolar field due to the sample is relatively intense reaching a magnitude $B^{\max}_{\text{spl}} = 0.6\mu_0 M^{(0)}_{\text{spl}}/(4\pi)$.

To more fully appreciate this result it is important to bear in mind that the dipolar field of a uniformly magnetized infinite layer vanishes [8,9]. This can be seen by considering a point located a distance d above the layer, whereby the dipolar field due to the nuclei in a central circle of radius $\sqrt{2}d$ is anti-parallel to the field generated by nuclei outside this circle. The exact cancellation upon the superposition of both contributions is a non-intuitive and somewhat fortuitous result: the dipolar field of each individual spin diminishes with the

[2] Given the well-known spatial dependence of the dipolar field due to a magnetized sphere, this assumption considerably simplifies the mathematical treatment. As will become apparent soon, however, the inclusion of a more extended region throughout the tip body does not represent a substantial factor in the analysis.

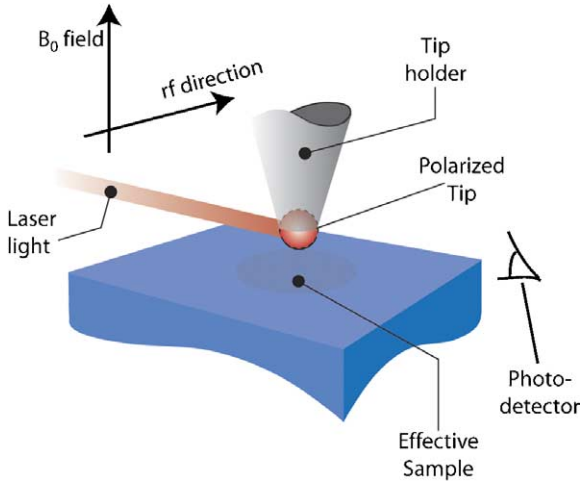

Fig. 1. Proposed experimental setup: a semiconductor tip is close to the surface of an extended sample. The system is immersed in a strong magnetic field pointing along the surface normal (z-axis). An RF coil (not displayed in the sketch) is used to manipulate the nuclear spin evolution both in the sample and in the tip. One or more laser beams are used to hyperpolarize the nuclei in the tip and optically probe its magnetization. To facilitate a formal description, it will be assumed that only a spherical region of radius a, equal to the radius of curvature of the tip, has been hyperpolarized. In practice, however, this condition is not necessary as the rest of the tip does not significantly contribute to the induced dipolar field on the sample.

distance to the center of the ring; however, the number of spins increases with the square of this distance. The nulling of the total dipolar field is the result of a delicate equilibrium involving regions of the sample that are far apart from each other. The magnetization distribution obtained for the case shown in Fig. 2A implies that, after the preparation sequence, only those nuclei within the central circle will contribute to the dipolar field in the tip. However, it is possible to alter the parameters of the preparation sequence to generate, for instance, a dipolar field of comparable magnitude, this time only due to nuclei outside the central circle (Fig. 2C) or in a ring around its center (Fig. 2B). This versatility and the almost optimum intensity of the induced dipolar field confer to this scheme very singular properties that can be used to selectively get information from complementary regions.

The detection of the sample magnetization by means of the tip is carried out in analogous fashion with that of the preparation period. Let us consider for this purpose the pulse sequence $(\theta)_y - t_{c2} - (\theta)_x$, this time applied at the resonance frequency of the nuclei within the semiconductor tip. Notice that the sample-tip contact time t_{c2} will be, in general, different from the one used during the preparation period and the tipping angle θ may differ

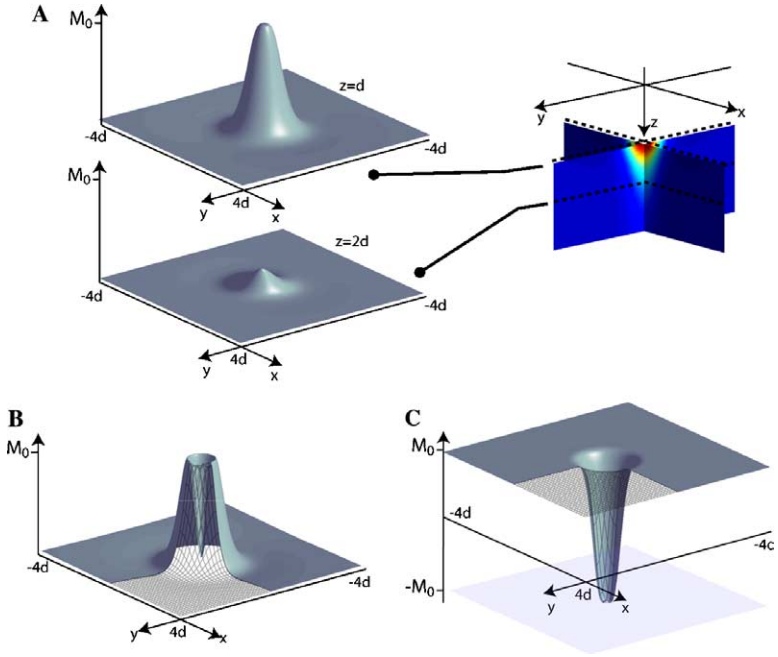

Fig. 2. Spatial distribution of the sample nuclear magnetization after evolution in the presence of the long-range dipolar field due to the tip. The polarized sphere in the tip is assumed to have its center located at the origin of the reference frame, a distance d above the surface of the sample. (A) Right: 3D localization of the nuclear spin alignment in the sample after an RF pulse sequence of the type $(\pi/2)_y - t_{c1} - (\pi/2)_x$. The inter-pulse interval has been chosen so that $\gamma_{\rm spl} t_{c1} B_{\rm tip}^{\rm max} = \pi/2$ (see text for notation). Left: spatial distribution of the magnetization on two separate planes. On the sample surface ($z = d$), the magnetization is essentially contained in a circle of radius $\sqrt{2}d$ and reaches maximum amplitude. As the distance to the tip increases, the magnetization rapidly vanishes. (B) Same as in (A) but with twice the evolution interval between the pulses. In this case only the surface plane has been displayed. The magnetization is still contained within a circle of radius $\sqrt{2}d$ but the central contribution has been removed, a situation that could be further exploited to improve resolution. For this case, the dipolar field induced by the sample reaches a magnitude $B_{\rm spl} \approx \mu_0 M_{\rm spl}^{(0)}/(4\pi)$. (C) Here, the phase of the second pulse in the preparation sequence was changed by 90° from x to y and the inter-pulse interval was chosen to be $\gamma_{\rm spl} t_{c1} B_{\rm tip}^{\rm max} = 1.06\pi$. On the surface plane, the magnetization is distributed so that only the region beyond a ring of radius $\sqrt{2}d$ contributes to the dipolar field $B_{\rm spl}$ at the tip. Notice that this is exactly the complement to the situation in (A). The sample dipolar field is in this case $B_{\rm spl} \approx -0.5\mu_0 M_{\rm spl}^{(0)}/(4\pi)$.

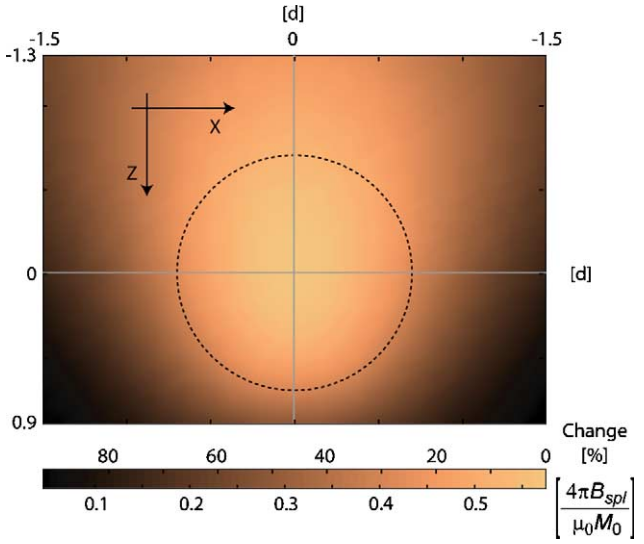

Fig. 3. Magnitude of the dipolar field in a vicinity of the tip after crafting the sample magnetization as in Fig. 2A. Positions have been expressed in units of the distance d; the center of the polarized sphere in the tip is at the origin. At this point, the dipolar field reaches its maximum equal to $0.6\mu_0 M_{\rm spl}^{(0)}/(4\pi)$. The dotted circle indicates the position of a (spherical) tip having a (curvature) radius $a = 0.7d$. Note that the dipolar field variation is slightly less than 30%.

from $\pi/2$. If, as before, we neglect all inter-spin interactions, the z-component of the magnetization in the tip at the end of the sequence is given by

$$\mathbf{M}_{\rm tip}^{(z)}(t_{c2}) = \mathbf{M}_{\rm tip}^{(0)}\left(1-\sin^2\theta\left(1-\sin\left(\frac{\pi}{2}\frac{(B_{\rm spl})_z}{\left(B_{\rm spl}^{\rm max}\right)_{\rm ref}}\right)\right)\right). \tag{3}$$

Here, the contact time t_{c2} has been chosen so that $\gamma_{\rm tip} t_{c2}(B_{\rm spl}^{\rm max})_{\rm ref} = \pi/2$. In this formula $(B_{\rm spl}^{\rm max})_{\rm ref}$ represents the (peak) dipolar field created by a reference sample (of optimum nuclear density) at the site of the tip. Formula [3] implies that at the end of the second time interval, the tip magnetization becomes modulated by the changes of the dipolar field $(B_{\rm spl})_z$, which, in turn, depends on the magnetization of the selected sample region. Thus, an optical inspection of the electronic spin precession in the semiconductor tip reveals a shift with respect to the Larmor frequency prior to manipulating the tip nuclei equal to

$$\Delta f = kM_{\rm tip}^{(0)}\sin^2\theta\left(1-\sin\left(\frac{\pi}{2}\frac{\langle M_{\rm spl}\rangle}{M_{\rm spl}^{\rm ref}}\right)\right). \tag{4}$$

For the case of Fig. 2A, $\langle M_{\rm spl}\rangle$ represents the average magnetization in a hemisphere of radius $\sim d$ located immediately close to the tip and $M_{\rm spl}^{\rm ref}$ is simply a scale factor interpreted as the magnetization in the same volume with best conceivable nuclear density (reference sample). Eq. (4) implies that, in principle, one can probe the local magnetization of the sample by optically inspecting the tip. Interestingly enough, the signal-to-noise ratio of the measurement only depends on our ability to detect changes of the electronic precession frequency in the semiconductor. This, in turn, rests on the amplitude of the nuclear magnetization in the tip and the electronic decoherence time; parameters that can be advantageously selected, as shown below.

Crucial in the detection scheme described so far is the adequate control of the short-range spin interactions that take place in a solid at the low temperatures necessary for optical pumping. A similar requirement is encountered in solid-state imaging [10] or in experiments that measure spin diffusion in a solid [11]. Here, multiple pulse coherent averaging is employed to suppress undesired spin–spin interactions during the creation of magnetization gratings by the pulsed field gradients. In the present case, the RF pulse sequence of Fig. 4 takes this condition into account: both during the preparation and encoding periods, the spin evolution takes place in the presence of homonuclear decoupling. On the other hand, an inversion π pulse at half each interval eliminates dephasing induced by heteronuclear interactions (dipolar, J-couplings) and local chemical shifts. Notice, however, that the effect due to the long-range dipolar field is preserved in both periods since the magnetizations in the sample and tip are synchronously inverted.

From a practical standpoint, the finite amplitude and spatial inhomogeneities of the radio-frequency (RF) field impose a limit to the time during which it is possible to preserve coherence in the spin evolution of a solid system. In static protonated samples, where the homonuclear dipolar interaction is particularly intense, this time is at most a few milliseconds (in a macroscopic sample) [12]. It follows from here that the modulation of the tip magnetization (and consequently, the detection sensitivity) will be optimized when the contact times between the tip and the sample are kept within this limit. The preparation time t_{c1} crucially depends on the magnetization and position of the tip relative to the sample: for the case considered in Fig. 2A, one has

$$t_{c1} = \frac{3\pi}{2}\left(\frac{d}{a}\right)^3\frac{1}{\mu_0\gamma_{\rm spl}M_{\rm tip}^{(0)}}. \tag{5}$$

In this expression we have included a factor 2 that addresses the nominal scaling incorporated in the majority of homonuclear decoupling sequences [12–15]. According to Eq. (5), the most favorable geometry is the one where the tip rests over the surface of the sample ($a \approx d$). An associated disadvantage is, however, that the dipolar field induced by the sample becomes inhomogenous within the tip volume. If the whole tip volume is used during the optical reading period, the tip must be separated from the sample surface, thus extending the contact time t_{c1}. The field map of Fig. 3 indicates that the spatial variation of $(B_{\rm spl})_z$ is about 30% throughout

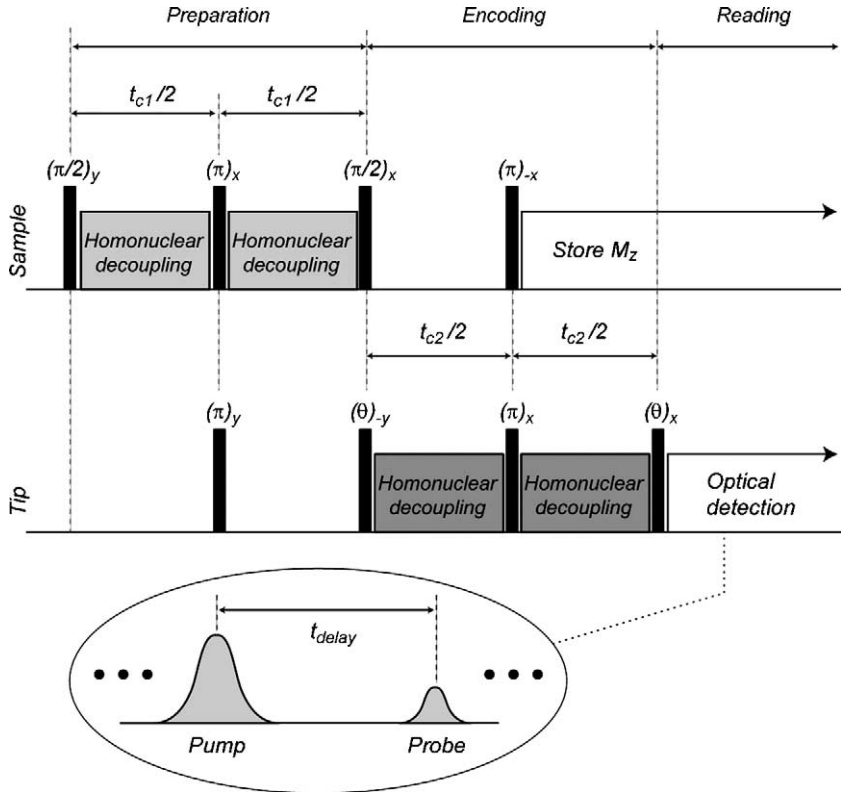

Fig. 4. Pulse sequence for the indirect detection of the sample magnetization. The part of the sample to be probed is selected during the initial *preparation* period. Here, a protocol equivalent to that of Fig. 2A has been followed. However, homonuclear decoupling is necessary to prevent decoherence due to inter-spin interactions. Dephasing due to local chemical shift or heteronuclear interactions is cancelled by the addition of a π-pulse at half the contact time t_{c1}. Notice that the effect due to the external long-range dipolar field is preserved by a simultaneous inversion of the tip magnetization. In the *encoding* period, the dipolar field due to the sample is used to modulate the magnetization in the tip. Again, RF decoupling and synchronous reversal of the magnetization are necessary to prevent undesired dephasing. Finally, an optical inspection of the tip magnetization is carried out during the *reading* period. This is accomplished by a train of time-delayed pump/probe laser pulses (see [5–7]).

a volume whose radius is slightly larger than half the distance to the surface ($a/d \approx 0.7$). As a simple numerical analysis demonstrates, a 30% change of the sample dipolar field over the tip volume only translates on a ~2% reduction of the electronic frequency shift range which, for most cases, does not represent a substantial problem. For this disposition and with a polarization of 10% (or 30%) in a GaAs tip, Eq. (5) yields $t_{c1} \approx 2$ ms (or 0.7 ms). Notice, however, that due to the cubic dependence with the distance, this value reduces to only ~700 μs (or 230 μs) when the tip rests just above the sample surface ($a \approx d$).[3] Such a disposition could be possible if the semiconductor tip is designed so that only the central fraction of its volume is used in the final period of optical reading. This could be implemented by altering the composition of the semiconductor to generate in the tip a core/shell structure analogous to that found in colloidal quantum dots [16–19]. With the laser frequency properly tuned during the reading period, only the central region can be monitored.

The contact time required during the encoding period t_{c2} is inversely proportional to the sample magnetization. For a spatial distribution similar to that of Fig. 2A, its value is given by the formula

$$t_{c2} \approx \frac{1}{\gamma_{\mathrm{tip}} B_{\mathrm{spl}}^{\max}}. \tag{6}$$

For a densely protonated sample in a magnetic field of 14 T (600 MHz proton frequency) and at 4 K, Eq. (6) yields $t_{c2} \approx 75$ ms. This value is still within the decoherence time of the nuclei in the semiconductor tip. This is because the comparatively lower value of the gyromagnetic ratio γ_{tip} leads to weaker dipolar interactions, which, accordingly, can be efficiently decoupled during longer times.

It is worth stressing that the role played by the sample magnetization in this scheme is merely to define the contact time necessary to modulate the tip magnetization. This is in striking contrast with the standard induction-based detection: if t_{c2} is kept within the optimum

[3] It has been assumed in this calculation that the dipolar field due to only one isotope of the tip (^{69}Ga, ^{71}Ga or ^{75}As) is effective throughout the preparation period. However, the contact time t_{c1} reduces approximately by a factor 1/3 if the dipolar field due to all three isotopes is controlled.

limits (<100 ms), the detection sensitivity does not depend on the sample magnetization but only on parameters associated with the semiconductor tip. One of these parameters is the tip magnetization, which determines the maximum amplitude or "scale" in the frequency shift of the electronic resonance frequency (Eq. (4)). Another key parameter is the electronic (transverse) relaxation time since it determines the resolution or "finesse" δf with which such changes can be read. For fixed values of t_{c1}, t_{c2}, and $M_{\mathrm{tip}}^{(0)}$, the minimum magnetization change that one can discern is inversely proportional to this time. For example, in GaAs at 5 K the electronic relaxation time is $\sim$2 ns implying that $\delta f \approx 0.25$ GHz. This value is significantly smaller than the maximum electronic frequency shift $\Delta f_{\max}$, which, for this example, is 10 GHz with a polarization of only 2% [5]. From here it can be seen that the following ratio holds: $\Delta f_{\max}/\delta f \approx 40$. Notice that $\Delta f_{\max} = kM_{\mathrm{tip}}\sin^2\theta$ indicating that it is possible to use shorter inspection pulses ($\theta < \pi/2$) at the expense of a larger polarization or a longer electronic decoherence time.

It is now realized that this scheme can be used to obtain an image of the sample: i.e., when the preparation period distributes the magnetization as in Fig. 2A, the resulting spatial resolution is defined by the distance d separating the center of curvature in the tip from the sample surface. This can be observed in Fig. 5, which displays the results of a simulation for three different values of d. The starting point for this simulation is the virtual (nuclear) spin distribution of Fig. 5A. Each pixel of this micrograph (350×520) represents a point-like magnetic moment having an amplitude proportional to the color of the image at the site. As the tip scans the sample, the dipolar field at the tip changes depend-

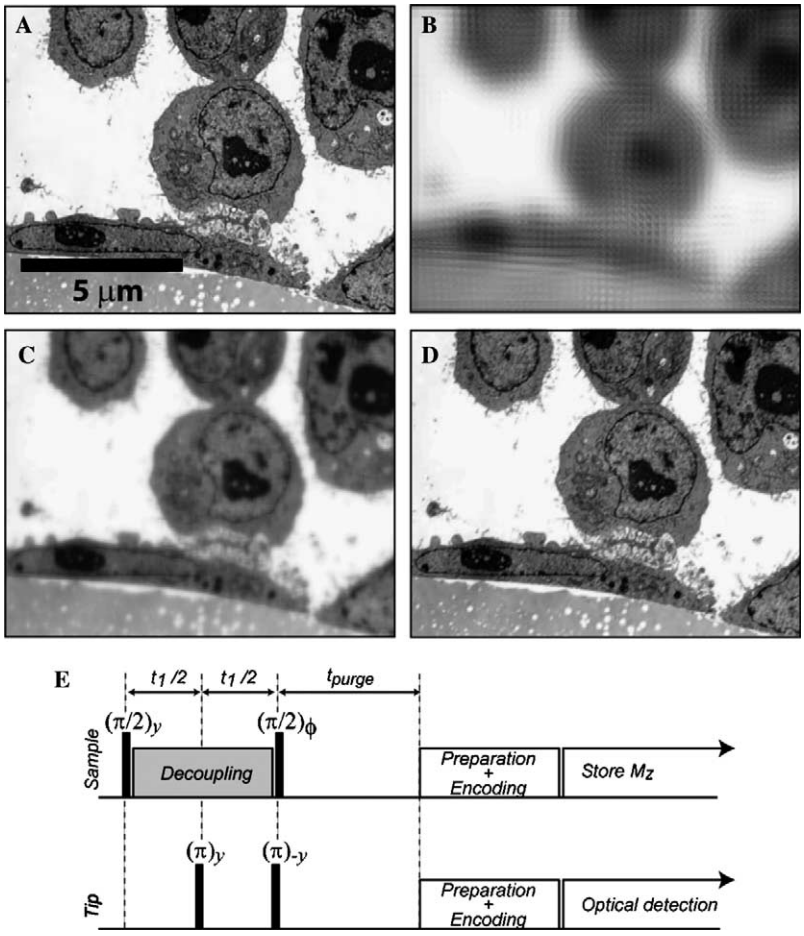

Fig. 5. (A) TEM image of cultured cells. The micrograph was used as a starting point of a numeric simulation in which each pixel represented a point-like magnetic dipole with intensity proportional to the spin density (gray scale) at the site. Following the preparation protocol of Fig. 2A, the local dipolar field B_{spl} was calculated as a (fictive) tip scanned the sample. For simplicity, the sample density was assumed constant along z; it was also assumed that, due to RF decoupling, spins evolved independently from their neighbors. The distance d from the center of the polarized tip to the surface of the sample was 0.8 μm in (B), 0.2 μm in (C), and 50 nm in (D). The ratio a/d was equal to 0.7 in all cases. (E) Pulse scheme for high-resolution local NMR spectroscopy. After an initial homogeneous excitation, the sample spins evolve over a variable period of time t_1 at the end of which a transverse component of the magnetization is stored. A purging time t_{p} longer than the (solid) transverse relaxation time is then used to destroy any remaining spin coherence. Finally, the detection protocol is carried out to selectively probe the sample. By incrementing t_1, the NMR FID can be reconstructed point-by-point; quadrature detection can be accomplished by cycling the phase of the second $\pi/2$-pulse from x to y.

ing on the sample density immediately close to it. Clearly, the resolution improves as the distance d (and, with it, the size of the tip) diminishes from almost 1 μm (Fig. 5B) to 50 nm (Fig. 5D).

An important point that should be stressed is that this method can be modified to also provide local spectroscopic information. Although there are several ways to approach this, Fig. 5E illustrates a simple case. Here, the sample evolves during an interval t_1 prior to the preparation period. By incrementing the length of t_1 in discrete steps it is possible to get the local nuclear resonance spectrum. Notice that the spin evolution during t_1 is unaffected by the presence of the external dipolar field because the tip magnetization is inverted at $t_1/2$. The scheme can also be extended to carry out multi-dimensional spectroscopy or to get selective images based on the chemical composition of the sample. Alternatively, it can be easily modified to introduce relaxation contrast. For the study of biological systems, this versatility could offer an appealing advantage compared to other methods such as magnetic force microscopy [20,21] where the presence of a strongly inhomogeneous magnetic field induced by the ferromagnetic tip prevents a high-resolution spectroscopic discrimination of the nuclei.

From a general perspective, the point-by-point reconstruction of the resonance spectrum does not significantly differ from the one used in other schemes of indirect detection. Recent examples are the encoding and "remote" detection of hyperpolarized xenon [22] or the reconstruction of nuclear magnetic resonance spectra detected by a mechanical oscillator in a "gradient-free" permanent magnet [23]. Notice that, in the presented method, the point-by-point reconstruction during the final optical reading period is not a significant inconvenience since the electronic relaxation is very fast ($\tau_{elec} < 1$ μs). On the other hand, because detection is carried out at low temperatures, long nuclear relaxation times (reaching in some cases several tens of minutes) do represent an important limitation that has to be taken into account. There are several tools that can be used to mitigate this problem: for example, for a given signal-to-noise ratio, the inspection angle θ in the tip diminishes the stronger the polarization is (or the longer the electronic relaxation time). It follows that, ideally, only a small fraction of the tip magnetization should be recovered after each observation. On the other hand, the addition of paramagnetic impurities could be used to control the sample relaxation although, in biological samples, proton relaxation is usually fast enough [24].

Mesoscopic effects due to dipolar interactions between nuclear spins in a magnetized system were observed for the first time almost 30 years ago [25]. However, remarkable applications in the area of liquid state NMR have rendered this area a topic of recent interest [26–29]. Here, it has been shown that, in principle, it is possible to manipulate long-range dipolar interactions to obtain local spectroscopic information and to reconstruct highly resolved images in solid systems at low temperatures. This technique, for which the name Dipolar Field Microscopy (DFM) is suggested, is based on the use of a hyperpolarized semiconductor micro-tip. After preparation and encoding periods, the optical reading of the electronic Larmor frequency in the semiconductor can be used to probe the sample magnetization in a region of the sample immediately close to the micro-tip. The spatial resolution is defined by the distance from the center of curvature of the tip to the sample surface. Crucial in this scheme is the decoupling of the short-range inter-spin interactions within the sample/tip during the preparation/encoding period respectively. When this condition is met, the sensitivity does not depend on the sample magnetization but only on parameters associated with the tip. Perhaps this is one of the most appealing aspects of a scheme that simultaneously incorporates the sensitivity of optical detection and the precise control of spin evolution, possible in modern NMR. Certainly, the practical implementation of this methodology presents important challenges. However, given the steady and fascinating progress in the area of nanotechnology, the viability of DFM appears quite promising.

Acknowledgments

C.A.M. gratefully acknowledges Prof. A. Pines and Dr. A. Trabesinger for inspiring discussions during the author's stay at UC Berkeley. The author is also indebted to Dr. K. Mackenzie for kindly providing the TEM image of Fig. 5A.

References

[1] B. Gross Levi, Progress made in near-field imaging with light from a sharp tip, Phys. Today 52 (1999) 18.
[2] S.W. Brown, T.A. Kennedy, D. Gammon, E.S. Snow, Spectrally resolved Overhauser shifts in single GaAs/Al_xGa_{1-x} As quantum dots, Phys. Rev. B 54 (1996) R17339–R17342.
[3] D. Gammon, S.W. Brown, E.S. Snow, T.A. Kennedy, Nuclear spectroscopy in single quantum dots: nanoscopic Raman scattering and nuclear magnetic resonance, Science 277 (1997) 85–88.
[4] See, for instance J.A. Marohn, P.J. Carson, J.Y. Hwang, M.A. Miller, D.N. Shykind, D.P. Weitekamp, Optical Larmor beat detection of high-resolution nuclear magnetic resonance in a semiconductor heterostructure, Phys. Rev. Lett. 75 (1995) 1364–1367.
[5] J.M. Kikkawa, D.D. Awschalom, All-optical magnetic resonance in semiconductors, Science 287 (2000) 473–476.
[6] S.A. Crooker, D.D. Awschalom, J.J. Baumberg, F. Flack, N. Samarth, Optical spin resonance and transverse spin relaxation in magnetic semiconductor quantum wells, Phys. Rev. B 56 (1997) 7574–7588.
[7] G. Salis, D.D. Awschalom, Y. Ohno, H. Ohno, Origin of enhanced dynamic nuclear polarization and all-optical nuclear

magnetic resonance in GaAs quantum wells, Phys. Rev. B 64 (2001) 195304.
[8] M.H. Levitt, Demagnetization field effects in two-dimensional solution NMR, Concepts Magn. Reson. 8 (1996) 77–103.
[9] A. Vlassenbroek, J. Jeener, P. Broekaert, Macroscopic and microscopic fields in high-resolution liquid NMR, J. Magn. Reson. Ser. A 118 (1996) 234–246.
[10] D.G. Cory, J.B. Miller, R. Turner, A.N. Garroway, Multiple pulse methods of 1H NMR imaging of solids: second averaging, Mol. Phys. 70 (1990) 331–345.
[11] W. Zhang, D.G. Cory, First direct measurement of the spin diffusion rate in a homogeneous solid, Phys. Rev. Lett. 80 (1998) 1324–1327.
[12] U. Haeberlen, High-Resolution NMR in Solids. Selective Averaging, Academic Press, New York, 1976.
[13] S.P. Brown, H.W. Spiess, Advanced solid-state NMR methods for the elucidation of structure and dynamics of molecular, macromolecular, and supramolecular systems, Chem. Rev. 101 (2001) 4125–4155.
[14] E. Vinogradov, P.K. Madhu, S. Vega, Strategies for high-resolution proton spectroscopy in solid-state NMR, Top. Curr. Chem. 246 (2004) 33–90.
[15] M.H. Levitt, A.C. Kolbert, A. Bielecki, D.J. Ruben, High-resolution ^{1}H NMR in solids with frequency-switched multiple pulse sequences, Solid State Nucl. Magn. Reson. 2 (1993) 151–163.
[16] M. Bruchez, J. Moronne, P. Gin, S. Weiss, A.P. Alivisatos, Semiconductor nanocrystals as fluorescent biological labels, Science 281 (1998) 2013–2016.
[17] B.O. Dabbousi, J. RodriguezViejo, F.V. Mikulec, J.R. Heine, H. Mattoussi, R. Ober, K.F. Jensen, M.G. Bawendi, (CdSe)ZnS core-shell quantum dots: synthesis and characterization of a size series of highly luminescent nanocrystallites, J. Phys. Chem. B 101 (1997) 9463–9475.
[18] X.G. Peng, M.C. Schlamp, A.V. Kadavanich, A.P. Alivisatos, Epitaxial growth of highly luminescent CdSe/CdS core-shell nanocrystals with photostability and electronic accessibility, J. Am. Chem. Soc. 119 (1997) 7019–7029.
[19] M.A. Hines, P. Guyot-Sionnest, Synthesis and characterization of strongly luminescent ZnS-capped CdSe nanocrystals, J. Phys. Chem. 100 (1996) 468–471.
[20] D. Rugar, O. Züger, S. Hoen, C.S. Yannoni, H.-M. Vieth, R.D. Kendrick, Force-detection of nuclear magnetic resonance, Science 264 (1994) 1560–1563.
[21] D. Rugar, C.S. Yannoni, J.A. Sidles, Mechanical detection of magnetic resonance, Nature 360 (1992) 563–566.
[22] A.J. Moulé, M.M. Spence, S.I. Han, J.A. Seeley, K.L. Pierce, S. Saxena, A. Pines, Amplification of xenon NMR and MRI by remote detection, Proc. Natl. Acad. Sci. USA 100 (2003) 9122–9127.
[23] G.M. Leskowitz, L.A. Madsen, D.P. Weitekamp, Force-detected magnetic resonance without field gradients, Sol. Stat. Nucl. Magn. Reson. 11 (1998) 73–83.
[24] M. Rosay, J.C. Lansing, K.C. Haddad, W.W. Bachovchin, J. Herzfeld, R.J. Temkin, R.G. Griffin, High-frequency dynamic nuclear polarization in MAS spectra of membrane and soluble proteins, J. Am. Chem. Soc. 125 (2003) 13626–13627.
[25] G. Deville, M. Bernier, J.M. Delrieux, NMR multiple echoes observed in solid ^{3}He, Phys. Rev. B 19 (1979) 5666–5688.
[26] W.S. Warren, S. Ahn, M. Mescher, M. Garwood, K. Ugurbil, W. Richter, R.R. Rizi, J. Hopkins, J.S. Leigh, MR imaging contrast enhancement based on intermolecular zero-quantum coherences, Science 281 (1998) 247–251.
[27] S. Warren, W. Richter, A.H. Andreotti, B.T. Farmer, Generation of impossible cross peaks between bulk water and biomolecules in solution NMR, Science 262 (1993) 2005–2009.
[28] W. Richter, S. Lee, W.S. Warren, Q. He, Imaging with intermolecular zero-quantum coherences in solution nuclear magnetic resonance, Science 267 (1995) 654–657.
[29] S. Vathyam, S. Lee, W.S. Warren, Homogeneous NMR spectra in inhomogeneous fields, Science 272 (1996) 92–96.